Journal of Physical Chemistry & Biophysics

Wu et al., J Phys Chem Biophys 2015, 5:6
DOI: 10.4172/2161-0398.1000196

Research Article Open Access

A DFT Study on the Degradation of Chlorobenzene to p-chlorophenol via Stable Hydroxo Intermediate Promoted by Iron and Manganese Monoxides

Yougen Wu[1], Yuchen Zhang[1] and Yanying Zhao[1,2]*

[1]*Department of Chemistry, Zhejiang Sci-Tech University, Hangzhou, China*
[2]*Engineering Research Center for Eco-dyeing and Finishing of Textiles, Key Laboratory of Advanced Textiles Materials and Manufacture Technology, Ministry of Education, Zhejiang Sci-Tech University, Hangzhou, China*

Abstract

The reaction paths for the conversion of chlorobenzene to *p*-chlorophenol are presented in detail using iron and manganese monoxides via the hydroxo insertion intermediate, HO–M–C_6H_4Cl (M=FeO, MnO). The molecular geometries and electronic structures for the reactants, intermediates, transition states, and products were optimized and analyzed in detail by density functional methods. The reaction potential surface profiles indicate that the metal-oxo species can activate the *para* C–H bond of the chlorobenzene to lead to the *p*-chlorophenol via the successive formation and the dissociation of the metal carbon bond, followed by removal of the metal atom (Fe or Mn). The intrinsic reaction co-ordinate (IRC) analyses indicated that no crossover point was searched for between the high-spin and low-spin potential energy surfaces; thus, no spin crossing was found between these two states potential energy surfaces. The low-spin potential energy surface lies above the high-spin one for the entire reaction pathway. Our theoretical study on the possible reaction pathways for the conversion of chlorobenzene to *p*-chlorophenol will also be useful for analyzing the catalytic functions of C–H bond activation and metal–carbon bond formation by transition metal complexes.

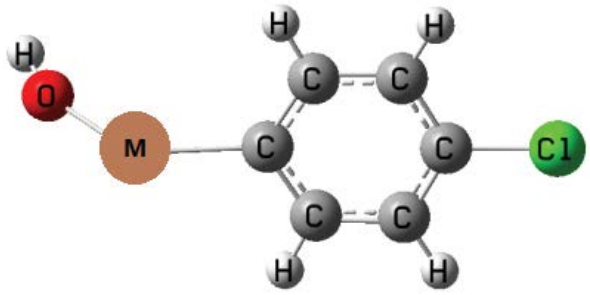

Stable hydroxo intermediates formed during the conversion of chlorobenzene promoted by transition-metal monoxides (M represents the Fe or Mn atom).

Keywords: *p*-chlorophenol; IRC analysis; Hydroxo intermediate; Reaction mechanism; DFT calculations

Introduction

Transition metals and their oxides are widely used as both catalysts and catalytic supports for C–H bond activation [1-5]. Nonetheless, these materials have not yet been fully investigated from a comprehensive mechanistic viewpoint [6]. The $CH_4 + MO^+ \rightarrow M^+ + CH_3OH$ reaction presents one of the simplest and earliest examples of C–H bond activation by transition metal compounds. Prior experimental studies have focused on gas-phase reactions of methane with first-row transition-metal oxide ions [2-10]. Considerable theoretical studies on these reactions have been conducted by Yoshizawa's group [11-13], who also performed the theoretical study on the reaction of FeO^+ with benzene [14,15]. In recent years, Andrew's group has reacted some of the group IV transition metal atoms with acetonitrile; although the observed experimental product CH_2=Zr(H)NC was assigned by matrix isolation infrared spectroscopy and isotopic substituted experiments combing with DFT frequency analysis, the detailed reaction mechanism was not took into account [16]. Further DFT theoretical calculations on the spin inversion process of the reaction pathway were reported by Jin et al. who considered two-state reactivity and spin-forbidden chemical reactions [17]. Besides the reactions of pure transition metal compounds with methane and acetonitrile, some small hydrocarbons such as C_2H_2, C_2H_4, and C_6H_6 [18-20] and halohydrocarbons such as CH_3Cl [21-24] have also been reported. However, the reactions of pure transition metal oxides with halogenated aromatic hydrocarbons have received very little attention.

Halogenated benzene compounds, one of the larger groups of anthropogenic materials, are widely used in the chemical and electronics industries. However, most of these compounds are hazardous organic pollutants because of their environmental impact and noxious effects, and are frequently found in various waste oils and other organic liquids. Recently, selective C–H activation with halo [25-27], cynao [28,29], and hydroxo [30-32] functional groups has attracted much attention in organic synthesis due to the possibility of incorporating versatile

***Corresponding author:** Yanying Zhao, Department of Chemistry, Zhejiang Sci-Tech University, Hangzhou, China, Tel: +86-571-86843627; E-mail: yyzhao@zstu.edu.cn

Received October 08, 2015; **Accepted** November 25, 2015; **Published** November 30, 2015

Citation: Wu Y, Zhang Y, Zhao Y (2015) A DFT Study on the Degradation of Chlorobenzene to p-chlorophenol via Stable Hydroxo Intermediate Promoted by Iron and Manganese Monoxides. J Phys Chem Biophys 5:196. doi:10.4172/2161-0398.1000196

functional groups. In these reactions, the functional groups remain unreactive under suitable conditions, thereby allowing the activation of the targeted C–H bonds to form more complicated organic molecules. In addition, hydroxylation of the halogenated benzenes is biologically important, because it forms *p*-substituted hydroxyhalobenzenes that are mostly found in mosquito larva and water extracts. Recently, group IX metals have been extensively reported for the activation of C–H bonds in the presence of carbon halide bonds. Milstein described an exclusive activation of *ortho* C–H bonds in chloro- and bromobenzene via the cationic pincer complex $[(PNP^*)Ir]^+$ (PNP,′-bis(di--butylphosphino)-2,6-diaminopyridine) [33]. Kinetic preference for C–H activation and thermodynamic preference for C–Cl activation for chlorobenzene (PhCl) was observed by Ozerov [34] by using an analogous $(PNP)Ir^I$ system and also in related DFT calculations by Hall [35].

In this paper, we report a theoretical study of the reactions of neutral MnO and FeO with chlorobenzene, taking spin multiplicities into consideration. The reaction intermediates and the energetics along the reaction pathway are computed and analyzed in detail. Our theoretical analysis on the direct hydroxylation of chlorobenzene will help the researchers in the fields of catalysis chemistry and bioinorganic chemistry.

Computational Methods

The computations were performed using the Gaussian 09 *ab initio* program package [36]. The 6-311++G(d, p) all-electron basis sets were used for all atoms [37,38]. To select an appropriate functional, different functionals (including B3LYP [39-41], M06 [42], M062X [42] and M11 [43]) were tested by calculating the M–O bond lengths and the M–O stretching vibrational frequencies of all first-row transition-metal monoxides (M=Sc to Cu). The results indicated that both wB97XD and B3LYP demonstrated the best results. Since B3LYP is a frequently reported functional, it was chosen to optimize the structures of the molecules under investigation. The first structures to be optimized were the equilibrium structures of PhCl, MnO, and FeO monomers, reactant complexes (PhCl)MO, hydroxo intermediates ClPh(MOH), product complexes, and their transition states with different multiplicities. Complete optimization of the molecular geometries was done with all stationary points. The harmonic vibrational frequencies of all the species were calculated with analytic second derivatives at the same level. This confirms that each stationary point is a local minimum or is a saddle point from systematic vibrational analyses of intrinsic reaction co-ordinates (IRCs) [44,45] and that it evaluates the zero-point vibrational energies (ZPVE). Each transition state was traced from a transition state toward both reactant and product directions along the imaginary mode of vibration using the algorithm developed by Gonzalez and Schlegel [46] in the mass-weighted internal coordinate system. Each IRC was constructed from 50 to 100 steps.

Results and Discussion

Potential energy diagram of the reaction between MO and C_6H_5Cl

DFT/B3LYP calculations were performed on the potential reaction products. Figures 1 and 2 shows the computed profiles of the potential energy surfaces for the reaction of transition metal monoxides with chlorobenzene in both the quartet and sextet states for MnO and in both the triplet and quintet states for FeO. Every possible computed structure of all intermediates and transition states is also displayed in Figures S1 and S2 (Provided in supplementary information). From the figures, we conclude that the chlorobenzene–*p*-chlorophenol reaction is a two-step reaction: in the first step, the compound passes through a transition state (TS1) to form a hydroxyl intermediate (HO-M-C_6H_4Cl); in the second step, another transition state (TS2) forms that leads to the product. Figure 1 shows that the computed potential energy profiles of the quintet states have lower energy than the triplet states for FeO. Figure 2 indicates that the energies of the sextet states are below that of the quartet states during the entire reaction process. All the triplet states lie above the quintet ones; therefore, we discuss only the quintet states here. The activation energies required to form TS1 from the reactant are 15.7 kcal/mol for MnO and 20.2 kcal/mol for FeO along the sextet and quintet states of the reaction coordinates. Two stable hydroxyl intermediates are also optimized. Notably, no spin crossing was detected for the entire reaction. With the help of B3LYP computation, the overall reaction is predicted to be exothermic for MnO, with the release of 4.4 kcal/mol of energy. In contrast, the reaction is endothermic for FeO, with the required energy being 14.4 kcal/mol.

IRC analyses

As shown in Figures 3-5, the quintet-state IRC analysis can be used to investigate the reaction intermediates and transition states for the FeO system. We begin with by investigating the first step-reaction using IRC analysis in which the reactant complex forms the intermediate through TS1. This first step-reaction can be viewed as a 1,3-hydrogen migration (Figure 1). This is the most important step for cleaving *p*-hydrogen that migrates to oxygen and finally forms a hydroxy intermediate, which combines with OH and C_6H_4Cl ligands. The first step-reaction in the quintet state has been discussed in detail in Figure 3, in which we present the change in the geometrical parameters during the reaction. The IRC was started from TS1 (s=0), which exhibits a C_s structure with an imaginary vibrational mode of 1678*i* cm^{-1}, toward both the reactant (s<0) and product (s>0) directions. In principle, both directions would lead to an energy minimum in the reactant or product "valleys." Unfortunately, the IRC ended before the true structure of the reactant complex could be acquired, although the terminal energy is very close to that of the reactant complex. However, this IRC analysis is good enough to increase our understanding of the reaction pathway.

The most important first step-reaction along the reaction pathway is discussed in detail in Figure 3a, in which the migrating hydrogen

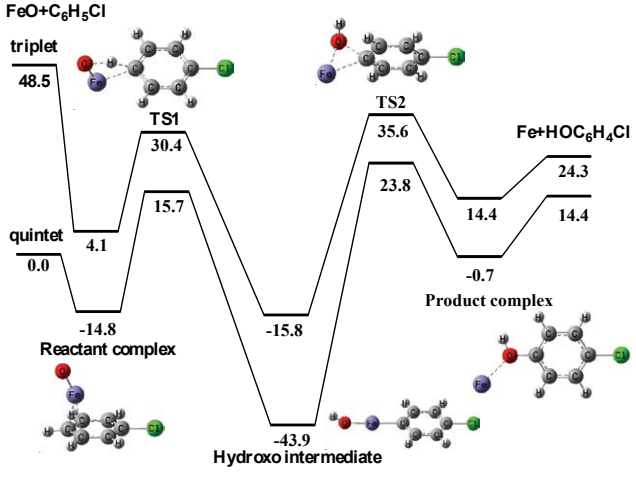

Figure 1: Potential energy diagram (including zero-point energy) along the reaction pathway, $FeO+C_6H_5Cl \rightarrow Fe+HOC_6H_4Cl$, in the quintet states. Relative energies are in kcal/mol.

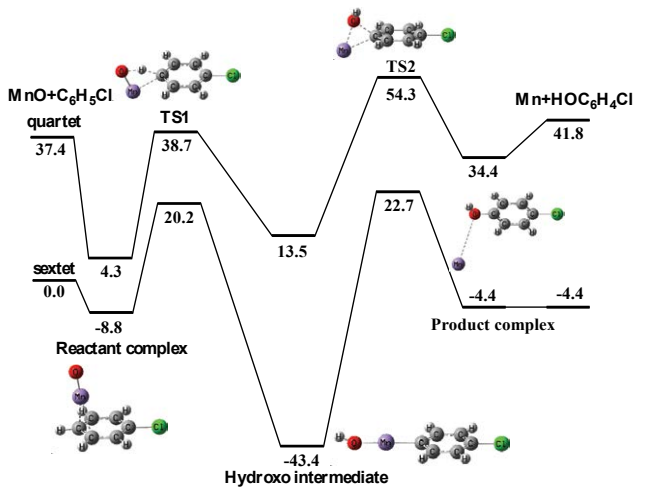

Figure 2: Potential energy diagram (including zero-point energy) along the reaction pathway, $MnO+C_6H_5Cl \rightarrow Mn+HOC_6H_4Cl$, in the sextet states. Relative energies are in kcal/mol.

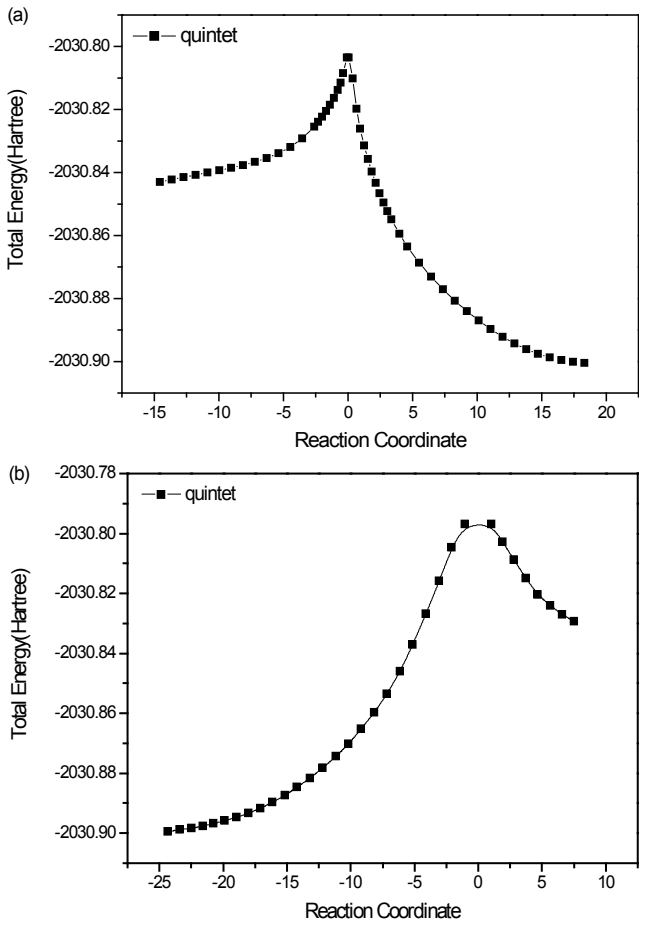

Figure 3: Fe compound potential energies along the quintet IRC (a) from the reactant complex to the hydroxo intermediate and (b) from the hydroxo intermediate to the product complex.

atom interacts not only with the C and O atoms, but also with the Fe atom to some extent. The Fe atom can significantly contribute to the migration of the H atom. It is obvious that the Fe–H distance exhibits an interesting feature; the distance reaches the minimum value (1.78 Å) in TS1. This means that there is an orbital overlap between the migrating hydrogen atom and the Fe atom in the vicinity of TS1. Therefore, the Fe atom must play an essential role in C–H bond dissociation. In addition, the Fe–O bond length does not change very much through the entire process.

Next, let us look at the change in the bond angle for the first step-reaction. In Figure 3b, the change in the C–Fe–O angle exhibits an interesting feature: the angle keeps changing and reaches the minimum value (75°) in TS1. The C–H bond begins to dissociate at s=-0.6 and the O–H bond distance is nearly constant (0.96 Å) after passing s=1.5. Therefore, we consider that H-atom migration happens in the range -0.6<s<1.5. The activation barrier for the first step-reaction clearly derives from C–H bond dissociation and the C–Fe–O strain energy. Hence, the potential energy change would result from the strain of the C–Fe–O angle inside the region s<-0.6 and s>1.5. Bending of the C–Fe–O angle would play a supportive part in the C–H bond dissociation and O–H bond formation.

After discussing the first step-reaction of the reaction pathway, let us now look at the second step-reaction. Here, the intermediate forms the product through TS2, which can be viewed as 1,2-*p*-chlorophenyl

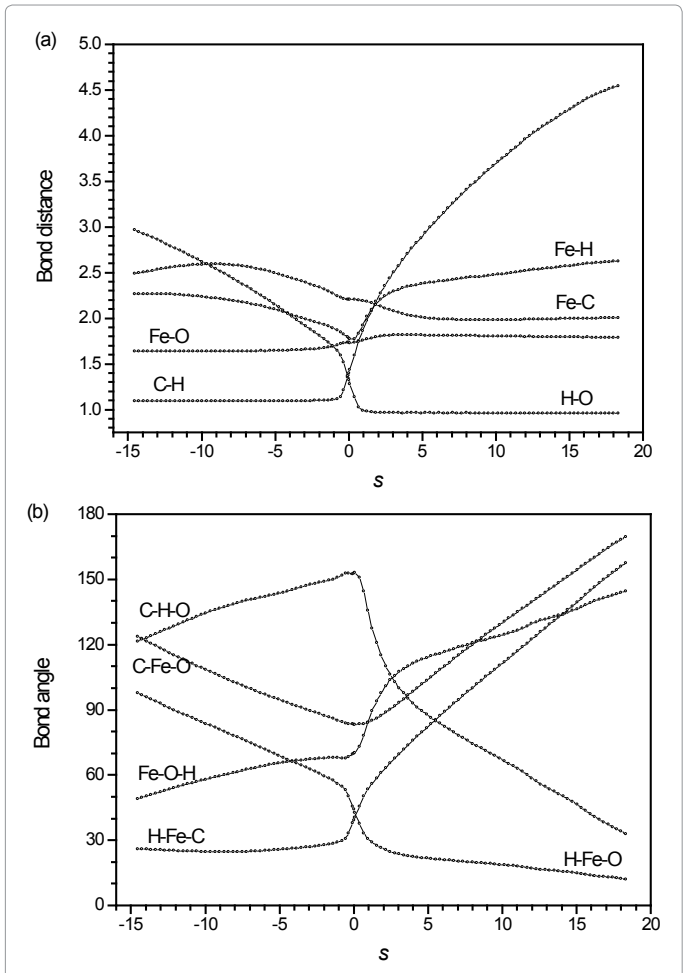

Figure 4: Change of internal coordinates for concerted C–H bond dissociation along the quintet IRC from the reactant complex to the hydroxo intermediate. Atomic distances are in Å and bond angles are in degrees.

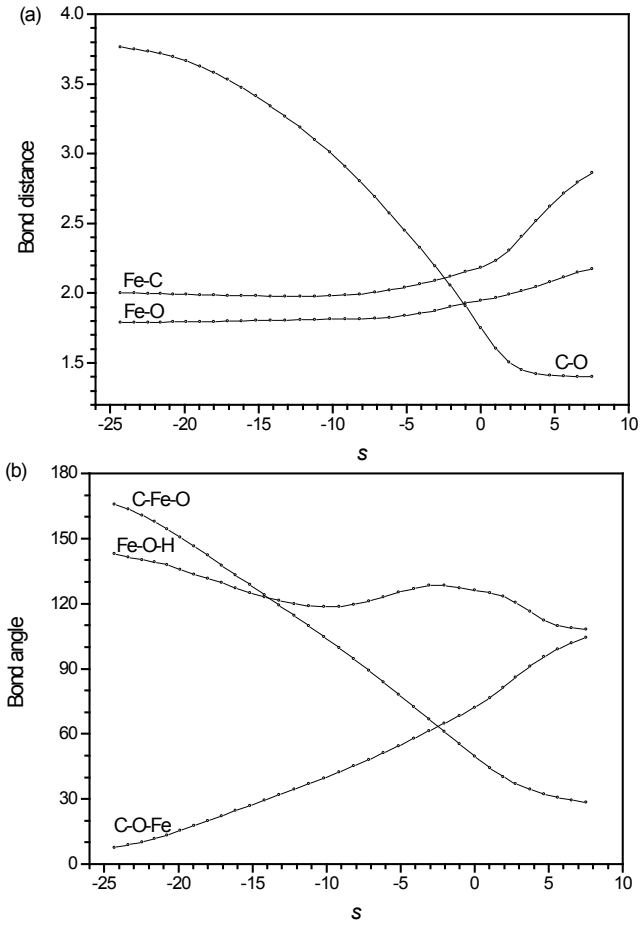

Figure 5: Change of internal coordinates for the concerted *p*-chlorophenyl migration along the quintet IRC from the hydroxo intermediate to the product complex. Atomic distances are in Å and bond angles are in degrees.

migration on the hydroxy intermediate (Figure 4). The IRC was started from TS2 (s=0), which exhibits a C_1 structure with an imaginary vibrational mode of 416*i* cm^{-1}, toward both the intermediate (s<0) and product complex (s>0) directions. Fortunately, this IRC analysis was successful. The most significant aspect in the second step-reaction is the dissociation of the Fe–C bond and formation of the C–O bond.

We similarly investigated the details of the MnO and C_6H_5Cl reaction process by using the IRC analysis method. Because all the quartet states lie above the sextet ones, we discuss only the sextet states here.

To begin with, we first take a look at the detailed IRC analyses. The sextet-state IRC analysis is correctly connected by the reaction intermediates and transition states, as can be seen in Figure 6. Firstly, we consider the IRC analysis for the first step-reaction, which involves the transition of the reactant complex to the intermediate through TS1. This step-reaction can be viewed as 1,3-hydrogen migration. This is the most important step for cleaving *p*-hydrogen that migrates to oxygen and finally forms the hydroxy intermediate made of OH and C_6H_4Cl ligands (Figure 7). The IRC was started from TS1 (s=0), which exhibits a C_s structure with an imaginary vibrational mode of 1733*i* cm^{-1}, towards both the reactant (s<0) and product (s>0) directions. In principle, both directions would lead to an energy minimum in the reactant or product "valleys." Unfortunately, similar to the case with FeO, our IRC ended before the true structure of the reactant complex could be achieved, although the terminal energy is very close to that of the reactant complex. Despite this, the IRC analysis considered in this study is sufficient to increase our understanding of the reaction pathway.

The most important first step-reaction along the reaction pathway is discussed in detail in Figure 7a. The migrating hydrogen atom interacts not only with the C and O atoms but also with the Mn atom to some extent. The Mn atom is not a spectator in the first step-reaction process; it also significantly contributes to the migration of the H atom. It is obvious that the Mn–H bond distance exhibits an interesting feature: the distance reaches the minimum value (1.85 Å) in TS1. This means that there is an orbital overlap between the migrating hydrogen atom and the Mn atom in the vicinity of TS1. Therefore, the Mn atom must play an essential role in this C–H bond dissociation. In addition, the Mn–O distance remains unchanged during the entire process.

Next, let us look at the change in the bond angle for the first step-reaction. In Figure 7b, the change in the C–Mn–O angle exhibits an interesting feature; the angle keeps changing and reaches the minimum value (79°) in TS1. The C–H bond starts to dissociate at *s*=-0.6 and the O–H distance remains nearly constant (0.96 Å) after passing *s*=1.0. Therefore, we consider that H-atom migration happens in the range -0.6<s<1.0. The activation barrier for the first step-reaction obviously derives from C–H bond dissociation and the C–Mn–O strain energy.

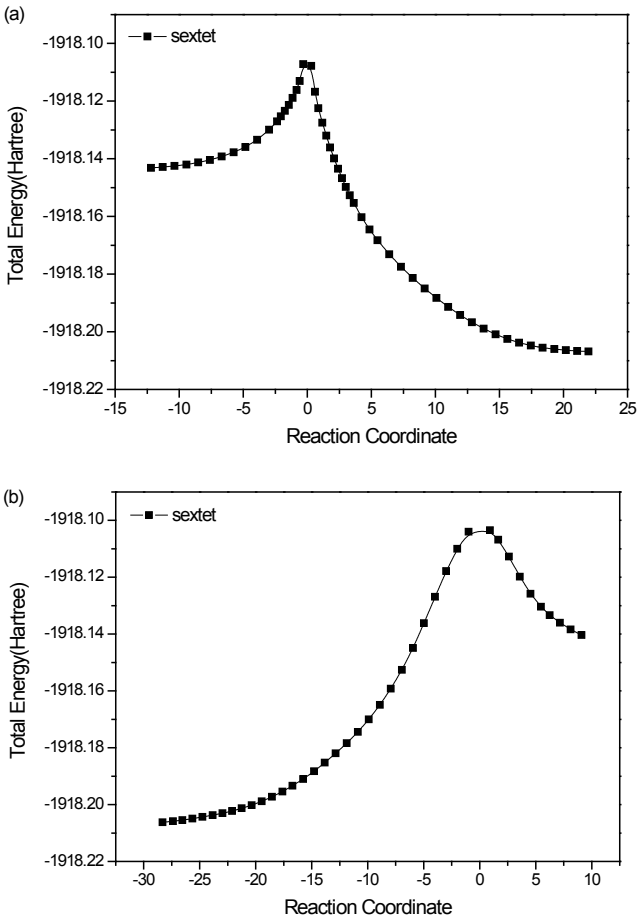

Figure 6: Mn compound potential energies along the sextet IRC (a) from the reactant complex to the hydroxo intermediate and (b) from the hydroxo intermediate to the product complex.

Hence, the potential energy change would result basically from the strain of the C–Mn–O angle inside the region s<-0.6 and s>1.0. Bending of the C–Mn–O angle would play a supporting role in C–H bond dissociation and O–H bond formation.

After discussing the first step-reaction of the reaction pathway, let us now look at the second step-reaction. In this section, the intermediate forms the product through TS2, which can be viewed as a 1,2-*p*-chlorophenyl migration on the hydroxy intermediate (Figure 8). The IRC was started from TS2 (s=0), which exhibits a C_1 structure with an imaginary vibrational mode of 368*i* cm^{-1}, toward both the intermediate (s<0) and product complex (s>0) directions. Fortunately, this IRC analysis was successful. The most significant aspect in the second step-reaction is the dissociation of the Mn–C bond and the formation of the C–O bond.

Conclusions

In this study, we have described the IRC analyses of the chlorobenzene→*p*-chlorophenol reaction by FeO and MnO. The geometries of the reactants, products, intermediates, and transition states along the reaction pathway via the important insertion intermediate, HO-M-C_6H_4Cl (M=FeO, MnO), have been described in detail for the quintet-state FeO and sextet-state MnO. A possible cross-point has been assumed to exist between the high-spin and low-spin potential energy surfaces. Nonetheless, no spin crossing between that two states' potential energy surfaces was found after computing both the triplet and quintet states for FeO and both the quartet and sextet states for MnO. The low-spin potential energy diagram lies above the high-spin one for the entire reaction pathway. We believe that our theoretical study on the possible reaction pathways for the conversion of chlorobenzene to *p*-chlorophenol will help in the analysis of catalytic and enzymatic functions of C-H and C-C bond activation by transition metal complexes.

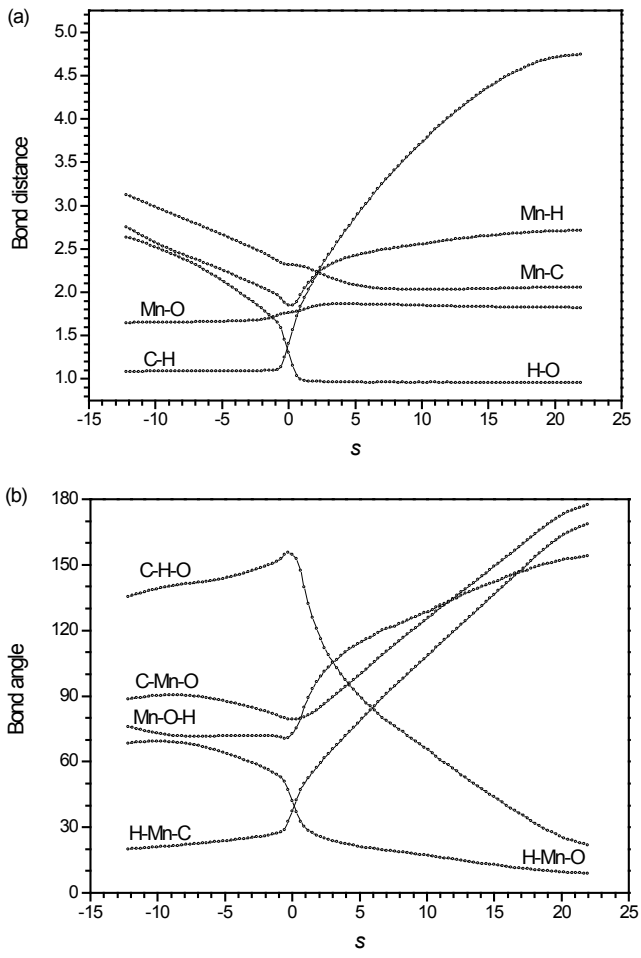

Figure 7: Change of internal coordinates for concerted C–H bond dissociation along the sextet IRC from the reactant complex to the hydroxo intermediate. Atomic distances are in Å and bond angles are in degrees.

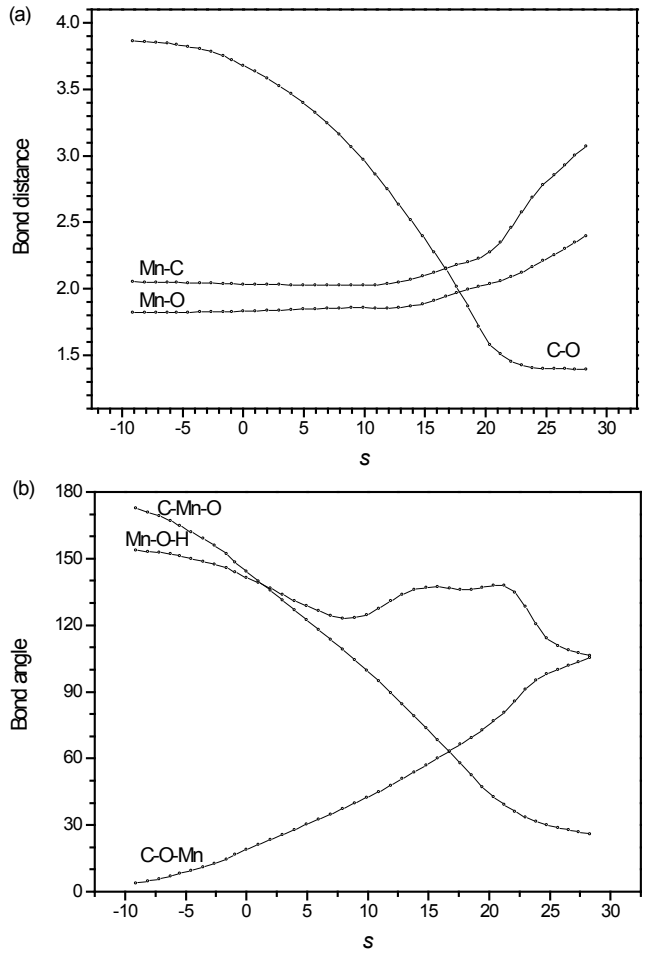

Figure 8: Change of internal coordinates for the concerted *p*-chlorophenyl migration along the sextet IRC from the hydroxo intermediate to the product complex. Atomic distances are in Å and bond angles are in degrees.

Acknowledgements

We gratefully acknowledge financial support from National Natural Science Foundation of China (Grants No. 21273202 and 21473162) and National Basic Research Program of China (2013CB834604). Zhao YY is grateful to the Project Grants 521 Talents Cultivation of Zhejiang Sci-Tech University. This work is also supported by Zhejiang Provincial Top Key Academic Discipline of Chemical Engineering and Technology. We also thank editage (http://www.editage.cn) assistance during the preparation of this manuscript.

References

1. Balcells D, Clot E, Eisenstein O (2010) C-H bond activation in transition metal species from a computational perspective. Chem Rev 110: 749-823.
2. Arockiam PB, Bruneau C, Dixneuf PH (2012) Ruthenium(II)-catalyzed C-H bond activation and functionalization. Chem Rev 112: 5879-5918.

3. Smalley AP, Gaunt MJ (2015) Mechanistic Insights into the Palladium-Catalyzed Aziridination of Aliphatic Amines by C-H Activation. J Am Chem Soc.
4. Mallick S, Rana S, Parida K (2011) Liquid Phase Hydrodechlorination of Chlorobenzene over Bimetallic Supported Zirconia Catalyst. Ind Eng Chem Res 50: 12439-12448.
5. Zhang L, Anderson WA (2013) Effect of Ozone and Sulfur Dioxide on the Photolytic Degradation of Chlorobenzene in Air. Ind Eng Chem Res 52: 3315-3319.
6. Zemski KA, Justes DR, Castleman AW (2002) Studies of Metal Oxide Clusters: Elucidating Reactive Sites Responsible for the Activity of Transition Metal Oxide Catalysts. J Phys Chem B 106: 6136-6148.
7. Schröder D, Schwarz H (1995) C-H and C-C Bond Activation by Bare Transition-Metal Oxide Cations in the Gas Phase. Angew Chem Int Ed 34: 1973-1995.
8. Clemmer DE, Aristov N, Armentrout PB (1993) Reactions of scandium oxide (ScO+), titanium oxide (TiO+) and vanadyl (VO+) with deuterium: M+-OH bond energies and effects of spin conservation. J Phys Chem 97: 544-552.
9. Chen YM, Clemmer DE, Armentrout PB (1994) Conversion of CH4 to CH3OH: Reactions of CoO+ with CH4 and D2, Co+ with CH3OD and D2O, and Co+(CH3OD) with Xe. J Am Chem Soc 116: 7815-7826.
10. Aguirre F, Husband J, Thompson CJ, Stringer KL, Metz RB (2002) Electronic spectroscopy of intermediates involved in the conversion of methane to methanol by FeO+. J Chem Phys 116: 4071-4078.
11. Yoshizawa K, Shiota Y, Yamabe T (1998) Methane−Methanol Conversion by MnO+, FeO+, and CoO+: A Theoretical Study of Catalytic Selectivity. J Am Chem Soc 120: 564-572.
12. Yoshizawa K, Shiota Y, Yamabe T (1999) Intrinsic reaction coordinate analysis of the conversion of methane to methanol by an iron-oxo species: A study of crossing seams of potential energy surfaces. J Chem Phy 111: 538-545.
13. Shiota Y, Yoshizawa K (2000) Methane-to-Methanol Conversion by First-Row Transition-Metal Oxide Ions: ScO+, TiO+, VO+, CrO+, MnO+, FeO+, CoO+, NiO+, and CuO+. J Am Chem Soc 122: 12317-12326.
14. Yoshizawa K, Shiota Y, Yamabe T (1999) Reaction Pathway for the Direct Benzene Hydroxylation by Iron−Oxo Species. J Am Chem Soc 121: 147-153.
15. Shiota Y, Suzuki K, Yoshizawa K (2005) Mechanism for the Direct Oxidation of Benzene to Phenol by FeO+. Organometallics 24: 3532-3538.
16. Cho HG, Andrews L (2010) Infrared spectra of CH(2)=Zr(H)NC, CH(3)-ZrNC, and eta(2)-Zr(NC)-CH(3) produced by reactions of laser-ablated Zr atoms with acetonitrile. J Phys Chem A 114: 891-897.
17. Jin YZ, Wang YC, Ji DF (2013) Theoretical investigation for the mediated activation of the C-CN in CH3CN by Zr atom in the gas phase. Comput Theor Chem 1011: 75-81.
18. Chen MH, Huang ZG, Zhou MF (2004) Matrix isolation infrared spectroscopic and theoretical study of the transition metal (Mn and Fe) dioxide-ethylene complexes. Chem Phys 384: 165-170.
19. Wang GJ, Chen MH, Zhao YY, Zhou MF (2006) Matrix isolation infrared spectroscopic and density functional theoretical study of the reactions of transition metal monoxide (ScO and TiO) with acetylene. Chem Phys 322: 354.
20. Zhao YY, Huang YF, Zheng XM, Zhou MF (2010) Preparation and Characterization of the Agostic Bonding Molecules between Metal and Chlorine from the Reactions of Niobium and Tantalum Monoxide and Dioxide Molecules with Monochloromethane in Solid Argon. J Phys Chem A 114: 5779-5786.
21. Huang Y, Zhao Y, Zheng X, Zhou M (2010) Matrix isolation infrared spectroscopic and density functional theoretical study of the reactions of scandium and yttrium monoxides with monochloromethane. J Phys Chem A 114: 2476-2482.
22. Huang Z, Zhang B, Wang Q, Yuan Y, Sun L (2016) Theoretical study of the reactions of transition-metal monoxides (Sc-V) with monochloromethane: Structures, energies and reaction mechanisms. Comput Theor Chem 1075: 1-8.
23. Zhao Y, Fan K, Huang Y, Zheng X (2013) Matrix isolation infrared spectra, assignment and DFT investigation on reactions of iron and manganese monoxides with CH3Cl. Spectrochim Acta A Mol Biomol Spectrosc 116: 96-101.
24. Zhao Y (2013) C-Cl activation by group IV metal oxides in solid argon matrixes: matrix isolation infrared spectroscopy and theoretical investigations of the reactions of MOx (M = Ti, Zr; x = , 2) with CH3Cl. J Phys Chem A 117: 5664-5674.
25. Tellers DM, Yung CM, Arndtsen BA, Adamson DR, Bergman RG (2002) Electronic and medium effects on the rate of arene C-H activation by cationic Ir(III) complexes. J Am Chem Soc 124: 1400-1410.
26. Ben-ari E, Cohen R, Gandelman M, Shimon LJW, Martin JML, et al. (2006) *ortho* C−H Activation of Haloarenes and Anisole by an Electron-Rich Iridium(I) Complex: Mechanism and Origin of Regio- and Chemoselectivity. An Experimental and Theoretical Study. Organometallics 25: 3190-3210.
27. Selmeczy AD, Jones WD, Partridge MG, Perutz RN (1994) Selectivity in the activation of fluorinated aromatic hydrocarbons by rhodium complexes [(C5H5)Rh(PMe3)] and [(C5Me5)Rh(PMe3)]. Organometallics 13: 522-532.
28. Heeres HJ, Meetsma A, Teuben JH (1990) CH Activation of Acetonitrile by Alkyl Compounds of the Early Lanthanoids: Dimeric Cyanomethyl-Lanthanoid Complexes with CH2CN Bridges. Angew Chem Int Ed Engl 29: 420-422.
29. Ittel SD, Tolman CA, English AD, Jesson JP (1978) The chemistry of 2-naphthyl bis[bis(dimethylphosphino)ethane] hydride complexes of iron, ruthenium, and osmium. 2. Cleavage of sp and sp3 carbon-hydrogen, carbon-oxygen, and carbon-halogen bonds. Coupling of carbon dioxide and acetonitrile. J Am Chem Soc 100: 7577-7585.
30. Lin M, Sen A (1994) Direct catalytic conversion of methane to acetic acid in an aqueous medium. Nature 368: 613-615.
31. Balaraman E, Khaskin E, Leitus G, Milstein D (2013) Catalytic transformation of alcohols to carboxylic acid salts and H2 using water as the oxygen atom source. Nat Chem 5: 122-125.
32. Owen JS, Labinger JA, Bercaw JE (2006) Kinetics and mechanism of methane, methanol, and dimethyl ether C-H activation with electrophilic platinum complexes. J Am Chem Soc 128: 2005-2016.
33. Ben-Ari E, Gandelman M, Rozenberg H, Shimon LJ, Milstein D (2003) Selective ortho C-h activation of haloarenes by an Ir(I) system. J Am Chem Soc 125: 4714-4715.
34. Fan L, Parkin S, Ozerov OV (2005) Halobenzenes and Ir(I): kinetic C-H oxidative addition and thermodynamic C-Hal oxidative addition. J Am Chem Soc 127: 16772-16773.
35. Wu H, Hall MB (2009) Carbon-hydrogen vs. carbon-halogen oxidative addition of chlorobenzene by a neutral iridium complex explored by DFT. Dalton Trans: 5933-5942.
36. Frisch MJ, Trucks GW, Schlegel HB, Scuseria GE, Robb MA, et al. (2009) Gaussian 09, Revision A.02; Gaussian Inc., Wallingford, CT.
37. Wachters JH (1970) Gaussian Basis Set for Molecular Wavefunctions Containing Third-Row Atoms. J Chem Phys 52: 1033.
38. Hay PJ (1977) Gaussian basis sets for molecular calculations. The representation of 3d orbitals in transition-metal atoms. J Chem Phys 66: 4377-4384.
39. Becke AD (1993) Density-functional thermochemistry. III. The role of exact exchange. J Chem Phys 98: 5648-5652.
40. Vosko SH, Wilk L, Nusair M (1980) Accurate spin-dependent electron liquid correlation energies for local spin density calculations: a critical analysis. Can J Phys 58: 1200-1211.
41. Lee C, Yang W, Parr RG (1988) Development of the Colle-Salvetti correlation-energy formula into a functional of the electron density. Phys Rev B Condens Matter 37: 785-789.
42. Zhao Y, Truhlar DG (2008) The M06 suite of density functionals for main group thermochemistry, thermochemical kinetics, noncovalent interactions, excited states, and transition elements: two new functionals and systematic testing of four M06-class functionals and 12 other functionals. Theor Chem Acc 120: 215-241.
43. Peverati R, Truhlar DG (2011) Improving the Accuracy of Hybrid Meta-GGA Density Functionals by Range Separation. J Phys Chem Lett 2: 2810-2817.
44. Fleurat-Lessard P, Ziegler T (2005) Tracing the minimum-energy path on the free-energy surface. J Chem Phys 123: 084101.
45. Fukui K (1981) The path of chemical reactions - the IRC approach. Acc Chem Res 14: 363-368.
46. Gonzalez C, Schlegel HB (1990) Reaction path following in mass-weighted internal coordinates. J Phys Chem 94: 5523-5527.
47. Liu Y, Wu W, Guan Y, Ying P, Li C (2002) FT-IR spectroscopic study of the oxidation of chlorobenzene over Mn-Based catalyst. Langmuir 18: 6229-6232.